

The population of hot subdwarf stars studied with *Gaia*

II. The *Gaia* DR2 catalogue of hot subluminous stars

S. Geier¹, R. Raddi², N. P. Gentile Fusillo³, and T. R. Marsh³

¹ Institut für Physik und Astronomie, Universität Potsdam, Haus 28, Karl-Liebknecht-Str. 24/25, D-14476 Potsdam-Golm, Germany

² Dr. Karl Remeis-Observatory & ECAP, Astronomical Institute, Friedrich-Alexander University Erlangen-Nuremberg, Sternwartstr. 7, D 96049 Bamberg, Germany

³ Department of Physics, University of Warwick, Coventry CV4 7AL, UK

Received Accepted

ABSTRACT

Based on data from the ESA *Gaia* Data Release 2 (DR2) and several ground-based, multi-band photometry surveys we compiled an all-sky catalogue of 39 800 hot subluminous star candidates selected in *Gaia* DR2 by means of colour, absolute magnitude and reduced proper motion cuts. We expect the majority of the candidates to be hot subdwarf stars of spectral type B and O, followed by blue horizontal branch stars of late B-type (HBB), hot post-AGB stars, and central stars of planetary nebulae. The contamination by cooler stars should be about 10%. The catalogue is magnitude limited to *Gaia* $G < 19$ mag and covers the whole sky. Except within the Galactic plane and LMC/SMC regions, we expect the catalogue to be almost complete up to about 1.5 kpc. The main purpose of this catalogue is to serve as input target list for the large-scale photometric and spectroscopic surveys which are ongoing or scheduled to start in the coming years. In the long run, securing a statistically significant sample of spectroscopically confirmed hot subluminous stars is key to advance towards a more detailed understanding of the latest stages of stellar evolution for single and binary stars.

Key words. stars: subdwarfs – stars: horizontal branch – catalogues

1. Introduction

Hot subdwarf stars (sdO/Bs) have spectra similar to those of main sequence O/B stars, but are subluminous and more compact. The formation and evolution of these objects is still unclear. In the Hertzsprung-Russell diagram hot subdwarfs are located at the blueward extension of the Horizontal Branch (HB), the so called Extreme or Extended Horizontal Branch (EHB, Heber et al. 1986) and are therefore considered to be core helium-burning stars (see Fig. 1).

To end up on the EHB, stars have to lose almost their entire hydrogen envelopes in the red-giant phase most likely via binary mass transfer. Consequently, hot subdwarfs turned out to be important objects to study close binary interactions and their companions can be substellar objects such as brown dwarfs, all kinds of main sequence stars, white dwarfs, and maybe even neutron stars or black holes (Maxted et al. 2001; Geier et al. 2010, 2011b; Kupfer et al. 2015; Kawka et al. 2015). Close hot subdwarf binaries with massive white dwarf companions are verification sources for gravitational wave detectors like LISA (Kupfer et al. 2018) and candidates for the progenitors of type Ia supernovae (Maxted et al. 2000; Geier et al. 2007; Geier et al. 2013). They are possibly ejected by such supernovae as hypervelocity stars (Geier et al. 2015a). Hot subdwarfs dominate old stellar populations in blue and ultraviolet bands. Their atmospheres are peculiar and can be used to study diffusion processes, such as gravitational settling or radiative levitation (O’Toole & Heber 2006; Geier 2013). Furthermore, several types of sdO/Bs are known to pulsate and turn out to be well suited for asteroseismic analyses

(e.g. Charpinet et al. 2011). For a comprehensive review of the state-of-the-art hot subdwarf research see Heber (2016).

SdO/B stars were initially found in surveys looking for faint blue stars at high Galactic latitudes (Humason & Zwicky 1947) and subsequently in larger-area surveys like the Tonantzintla survey (TON, Iriarte & Chavira 1957; Chavira 1958, 1959), the Palomar Haro Luyten survey (PHL, Haro & Luyten 1962), and the Palomar-Green (PG) survey (Green et al. 1986). The Kitt Peak-Downes (KPD) survey covered parts of the Galactic plane for the first time (Downes 1986). Kilkenny et al. (1988) published the first catalogue of spectroscopically identified hot subdwarf stars, which contained 1225 sdO/Bs.

More hot subdwarfs have been discovered subsequently in spectroscopic surveys like the Hamburg Quasar Survey (HS, Hagen et al. 1995), the Hamburg ESO survey (HE, Wisotzki et al. 1996), the Edinburgh-Cape Survey (EC, Kilkenny et al. 1997) and the Byurakan surveys (FBS, SBS, Mickaelian et al. 2007, 2008). Østensen (2006) compiled the hot subdwarf database containing more than 2300 stars.

Since then the number of known hot subdwarfs again increased. Especially, the Sloan Digital Sky Survey (SDSS) provided spectra of almost 2000 sdO/Bs (Geier et al. 2015b; Kepler et al. 2015, 2016). New samples of hot subdwarfs have also been selected from the EC survey and the GALEX all-sky survey photometry in the UV (e.g. Vennes et al. 2011). Furthermore, large-area photometric and astrometric surveys have been conducted in multiple bands from the UV to the far infrared. Combining these data, Geier et al. (2017) compiled an updated catalogue of 5613 hot subdwarf stars.

Send offprint requests to: S. Geier,
e-mail: sgeier@astro.physik.uni-potsdam.de

2. The catalogue of known hot subdwarf stars

In addition to the hot subdwarfs classified as sdO/B from the database of Østensen (2006), which was fairly complete up to the date of publication, Geier et al. (2017) added the subdwarf candidates from the FBS survey (Mickaelian et al. 2008), the sample of hot subdwarfs identified in the course of the Kepler mission (Østensen et al. 2010), the large sample of sdO/Bs spectroscopically identified from the Sloan Digital Sky Survey (SDSS) DR7 during the MUCHFUSS project (Massive Unseen Companions to Hot Faint Underluminous Stars from SDSS, Geier et al. 2015b), an unpublished sample of spectroscopically classified sdO/Bs selected from SDSS DR8-10, the sdO/B candidates from SDSS DR12 (Kepler et al. 2016), the candidate sample from SDSS DR10 classified as narrow-line hydrogen stars (NLHS) by Gentile Fusillo et al. (2015), the large sample of sdO/Bs from the complete EC survey (Kilkenny et al. 1997; O’Donoghue et al. 2013; Kilkenny et al. 2015, 2016), a sample of several hundred sdO/Bs selected from GALEX, GSC, and 2MASS photometry by R. H. Østensen and E. M. Green classified via follow-up spectroscopy, the sample of sdO/Bs selected from the Guide Star and the Galaxy Evolution Explorer (GALEX) catalogs by Vennes et al. (2011), the samples of Oreiro et al. (2011) and Perez-Fernandez et al. (2016) selected using Virtual observatory tools and multiband photometry, and the first sample of sdO/Bs discovered by the Large Sky Area Multi-Object Fibre Spectroscopic Telescope (LAMOST) survey (Luo et al. 2016).

Adding multi-band photometry, ground based proper motions and light curves from diverse surveys, Geier et al. (2017) cleaned this spectroscopic catalog and introduced a general classification scheme based on spectra and colour-indices. However, due to the limited coverage and complicated selection biases of the samples included in the catalogue, it was far from being complete and very inhomogeneous.

To study the diverse populations of hot luminous stars, an unbiased, all-sky sample of those objects is needed. The *Gaia* mission Data Release 2 (*Gaia* collaboration 2018a) now provides us with the data needed to achieve this for the first time. Here we present the first all-sky catalog of hot subluminous star candidates based on *Gaia* DR2.

3. Constructing the *Gaia* catalogue

The European Space Agency (ESA) astrometric mission *Gaia* measures positions, parallaxes, and proper motions for the about 1% of the stars in the Galaxy visible from Earth down the *Gaia* G magnitudes of ~ 20.7 mag (*Gaia* Collaboration et al. 2016). The first data release from the *Gaia* mission has been published by *Gaia* collaboration (2016). However, due to yet uncorrected chromatic effects, the bluest objects were excluded and only approximately 60 stars of the hot subdwarf catalogue by Geier et al. (? are part of the bright TGAS sample (Tycho-*Gaia* astrometric solution, Michalik et al. 2015) with preliminary parallaxes and proper motions, almost all of them composite sdB binaries.

By contrast, *Gaia* Data Release 2 (DR2; *Gaia* Collaboration et al. 2018a) is more complete by orders of magnitude, and it provides precise astrometry (Lindgren et al. 2018) as well as integrated photometry from the blue and red spectro-photometers G_{BP} (3300 – 6800 Å), G_{RP} (6400 – 10000 Å), and G (3300 – 10000 Å) passband photometry (Evans et al. 2018, see Fig. 1).

Using TOPCAT (Taylor 2005), we first cross-matched the hot subdwarf catalogue from Geier et al. (2017) with *Gaia* DR2 to see where the known hot subluminous stars are located in the *Gaia* parameter space. From this exercise we derived empirical

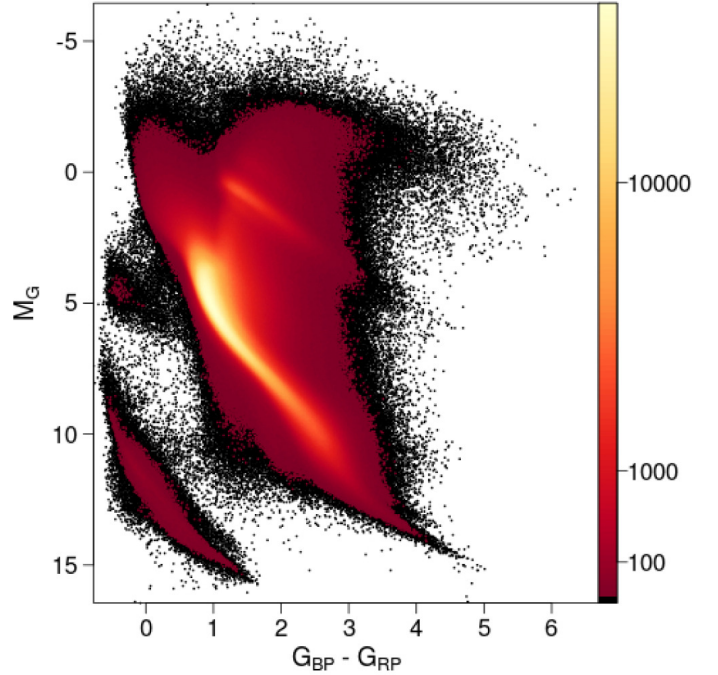


Fig. 1. Colour-absolute magnitude diagram taken from *Gaia* collaboration (2018b). The colour scale represents the square root of the relative density of stars. The hot subluminous stars are located blueward of the main sequence at absolute magnitudes around $M_G \sim 5$ mag.

selection criteria, which we adopted to select the full *Gaia* catalogue of hot subluminous stars from the *Gaia* data as outlined in the following sections. We also refined our selection based on lessons learned from the compilation of the *Gaia* DR2 catalogue of white dwarfs most recently published by Gentile Fusillo et al. (2018) and attempted to reduce the likely overlap with the white dwarf cooling sequence.

3.1. *Gaia* colour cut

Hot subluminous stars have colours similar to main sequence stars of spectral type O and B. In the *Gaia* colour space the sdO/B stars compiled by Geier et al. (2017) occupy the region $-0.7 < G_{BP} - G_{RP} \lesssim 0.7$, where single stars are located at $G_{BP} - G_{RP} \lesssim 0.0$ and the composite binaries with cool main sequence companions are found in the redder region (see Fig. 2, left panel).

To avoid significant contamination with WDs and low-mass main-sequence (MS) stars, we restricted the input sample for this catalogue to objects with $G < 19$ mag and $G_{BP} - G_{RP} < 0.7$. MS stars of spectral type M are both faint and numerous especially in dense regions around the Galactic plane. Due to their faintness and intrinsically very red colours, photometry in the G_{BP} passband is often so poor, that the $G_{BP} - G_{RP}$ colour index appears to be very negative mimicing a faint blue object. The same systematics can be seen for cool WDs. Numerous stars with unrealistically negative $G_{BP} - G_{RP}$ are found in the *Gaia* catalogue for G magnitudes close to the detection limit.

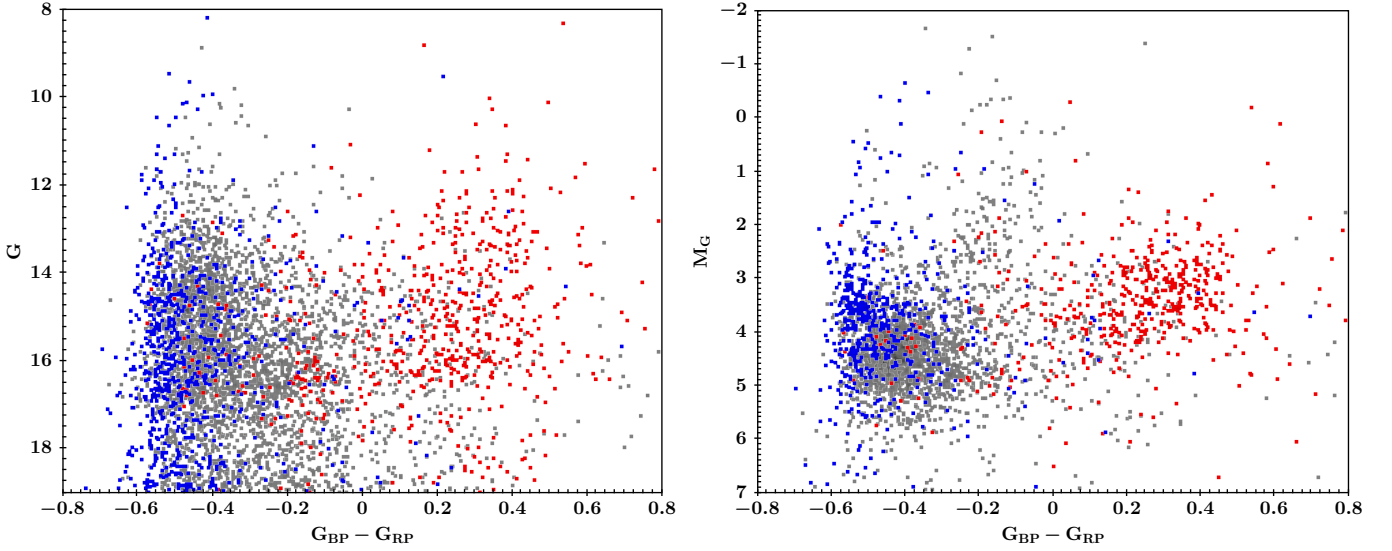


Fig. 2. Left panel: *Gaia* colour-magnitude diagram of the sdO/B stars with spectroscopic classification from the catalogue of Geier et al. (2017): SdB and sdOB type (grey), sdO type (blue), sdO/B composite binaries with cool main-sequence companions (red). Right panel: *Gaia* colour-absolute magnitude diagram.

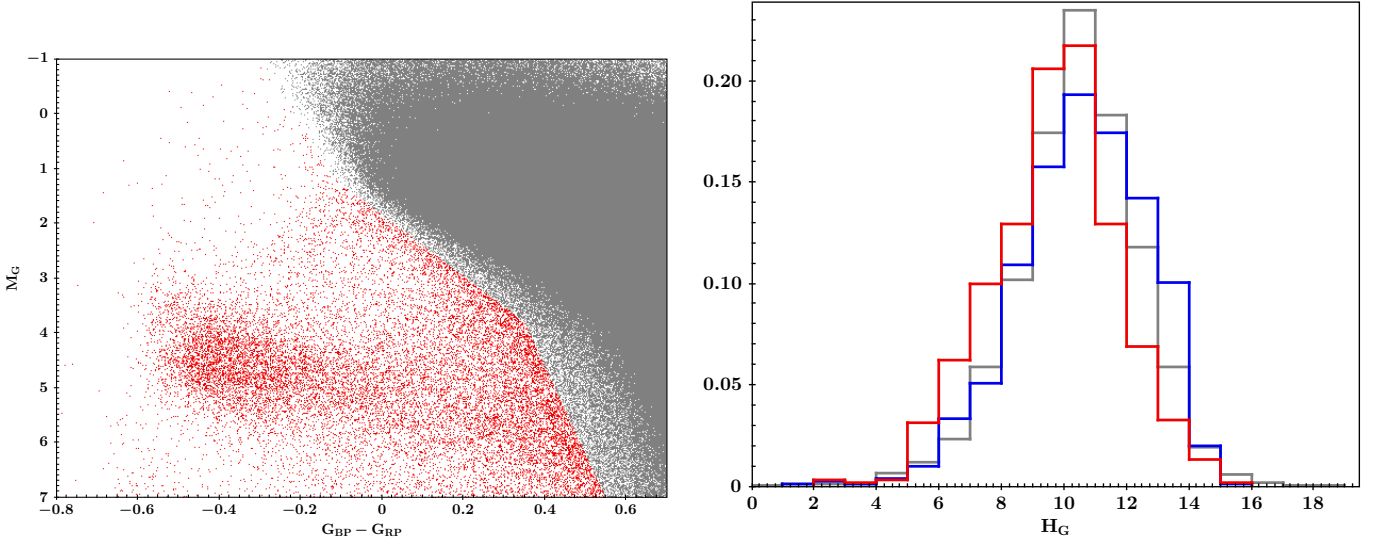


Fig. 3. Left panel: *Gaia* colour-absolute magnitude diagram. The selected objects are plotted in red. Right panel: Normalized reduced proper motion histogram of the sdO/B stars with spectroscopic classification from the catalogue of Geier et al. (2017): SdB and sdOB type (grey), sdO type (blue), sdO/B composite binaries with cool main-sequence companions (red).

3.2. Absolute magnitude selection

The ground-breaking nature of the *Gaia* mission is related to its performance in measuring stellar parallaxes for stars far beyond the solar neighbourhood. It is straightforward to calculate the absolute magnitude of a star by combining its apparent magnitude with a precise parallax determination. Absolute magnitudes and colours can then be used to disentangle hot subluminous stars from the much more luminous MS stars and the much less luminous hot WDs (see Fig. 1).

Applying a colour-cut $G_{BP} - G_{RP} < 0.7$, we selected all stars from *Gaia* DR2 with $G < 19$ mag with a parallax (π) uncertainty e_{PLX} better than 20% and selected only stars with absolute magnitudes $M_G = G + 5 \times (\log \pi + 1)$ typical for sdO/B stars. Fig. 2 (right panel) shows the absolute *Gaia* DR2 magnitudes of 5003

objects from the hot subdwarf catalogue from Geier et al. (2017), which have spectroscopic classifications. Based on this figure, we selected 2 750 896 objects with $-1.0 < M_G < 7.0$ mag.

To further select hot subluminous stars and filter out the main sequence, we applied the following empirically derived cuts to this sample:

$$\begin{aligned}
 M_G \leq 1.0 \text{ mag} : & \quad M_G \geq 11.76 \times (G_{BP} - G_{RP}) + 2.53 \\
 1.0 < M_G \leq 3.8 \text{ mag} : & \quad M_G \geq 5.6 \times (G_{BP} - G_{RP}) + 1.84 \\
 M_G > 3.8 \text{ mag} : & \quad M_G \geq 16 \times (G_{BP} - G_{RP}) - 1.8
 \end{aligned}$$

Table 1. Colour-selection

SDSS	$u - g < 0.7$ $g - r < 0.1$
SkyMapper	$u - g < 1.0$ $g - r < 0.4$
GALEX/APASS	$NUV - g < 2.0$
GALEX/PS1	$NUV - g < 1.7$ $g - r < 0.3$

Table 2. Colour-selection statistics

	total number	removed
SDSS	7037	1554
SkyMapper	21077	4852
GALEX/APASS	8530	2265
GALEX/PS1	16798	7730

This selection resulted in 18 221 objects. Fig. 3 (left panel) shows the selected sample. To make sure that the selection includes as many composite sdB binary candidates as possible, we carefully shifted the red edges of the selection area gradually and stopped as soon as the number of objects increased drastically as consequence of the contamination from main sequence stars.

3.3. Reduced proper motion selection

The absolute magnitude selection is only applicable to stars with good parallaxes and distances of less than $\sim 1 - 2$ kpc from the Sun. However, the majority of the known sdO/B stars are located further away. To select a sample of candidate hot subluminous stars at larger distances, we use the reduced proper motion as proxy for the distance and selection criterion. Gentile Fusillo et al. (2015) showed that this selection method is well suited to separate hot subdwarf from white dwarf candidates.

Fig. 3 (right panel) shows the distribution of the reduced proper motions in the G-band for the stars from the hot subdwarf catalogue (Geier et al. 2017). Based on this distribution we selected stars with reduced proper motions $H_G = G + 5(\log \mu + 1)$ between 5 and 15 (μ total proper motion). Due to the high contamination from main sequence stars we restricted our colour selection in this case to objects with $G_{BP} - G_{RP} < -0.05$. At low Galactic latitudes ($-20^\circ < b < 15^\circ$) we imposed another colour criterion $G_{BP} - G_{RP} > -0.7$ to exclude cool M dwarfs or brown dwarfs with low flux in the G_{BP} -band, which are more numerous in the dense region around the Galactic plane (Gaia collaboration 2018b; Evans et al. 2018).

The reduced proper motion selection yielded unphysically too many objects in the direction of the Large and Small Magellanic clouds (LMC and SMC), which are very dense and contain many hot and massive stars in the selected colour range. Since the astrometry of the sources in these regions might be affected by systematics, we cut out the sky region around the LMC and SMC from our selection. After removing the contaminant sources, we were left with 61 812 stars.

3.4. Multi-band photometry cleaning

As can be seen in Fig. 2 the *Gaia* passbands are too broad and red to allow for a temperature-sensitive colour-selection comparable to that provided by SDSS photometry (Geier et al. 2011a, 2017). To improve the target selection and remove stars with spectral types later than B, we cross-matched our sample with large-area, multi-band photometric catalogues, some of which only became available very recently.

Due to incompleteness, we did not use the cross-matches provided by *Gaia* DR2. Instead, we selected the closest matching sources adopting a radius of 5 arcsec and the epoch J2000 coordinates for the *Gaia* targets provided by CDS. Since hot subluminous stars have significantly lower proper motions than white dwarfs, mismatches due to stellar motion are negligible.

NUV and *FUV* photometry were taken from the GALEX DR6/7 (Bianchi et al. 2011) and restricted to sources with good photometry. We removed measurements with bad quality flags *nuv_artificat*, *fuv_artifact* of 2,8,10, and > 128 . Optical photometry was obtained from the AAVSO Photometric All Sky Survey (APASS DR9, Henden et al. 2016) in the *VBgr*-bands, the Sloan Digital Sky Survey DR12 (Alam et al. 2015) in the *ugriz*-bands (restricted to sources with quality flag Q smaller than 1), the Panoramic Survey Telescope and Rapid Response System (Pan-STARRS) PS1 survey (Chambers et al. 2016) in the *grizy*-bands, and the SkyMapper Southern Sky Survey DR1.1 (Wolf et al. 2018) in the *uvgriz*-bands.

We based our empirical selection on comparison with the colours of known hot subdwarfs from the Geier et al. (2017) catalogue. Fig. 4 shows the colour-colour diagrams and the selection criteria are provided in Table 1.

The fraction of objects removed by this selection (see Table 2) ranged from 22% to 27%. Only the GALEX/PS1 selection removed as many as 46% of the pre-selected objects. The reason for this is the larger coverage of the Galactic plane by the PS1 survey, where more sources are affected by blending and reddening.

3.5. Crowded region cleaning

Since our selection includes many sources in dense regions close to the Galactic plane, additional quality criteria must be imposed to remove blends and objects with bad astrometry (see Gentile Fusillo et al. 2018). To achieve this, we first made use of quality flags provided by *Gaia* DR2. The most important ones for our selection are *phot_bp_rp_excess_factor*, *astrometric_sigma5d_max* and *astrometric_excess_noise*.

The value of *phot_bp_rp_excess_factor* ($(f_{BP} + f_{RP})/f_G$, where f is the flux the respective passbands) indicates whether the *Gaia* bands are consistent with an isolated source and can be used to flag objects with unreliable colours or bright sky background (Evans et al. 2018). *astrometric_sigma5d_max* is a five-dimensional equivalent to the semi-major axis of the *Gaia* position error ellipse and indicates where one of the parameters is particularly bad (Lindgren et al. 2018).

astrometric_excess_noise is a measure of the residuals in the astrometric solution for the source. It can be used to identify single objects with unreliable parallax measurements, but might also indicate the presence of unresolved companions in astrometric binary systems (Lindgren et al. 2018).

The astrometric quality flags of our selection indicate a high quality of the derived parameters. The mean value of *astrometric_sigma5d_max* is 0.83 ± 0.31 with the maximum at

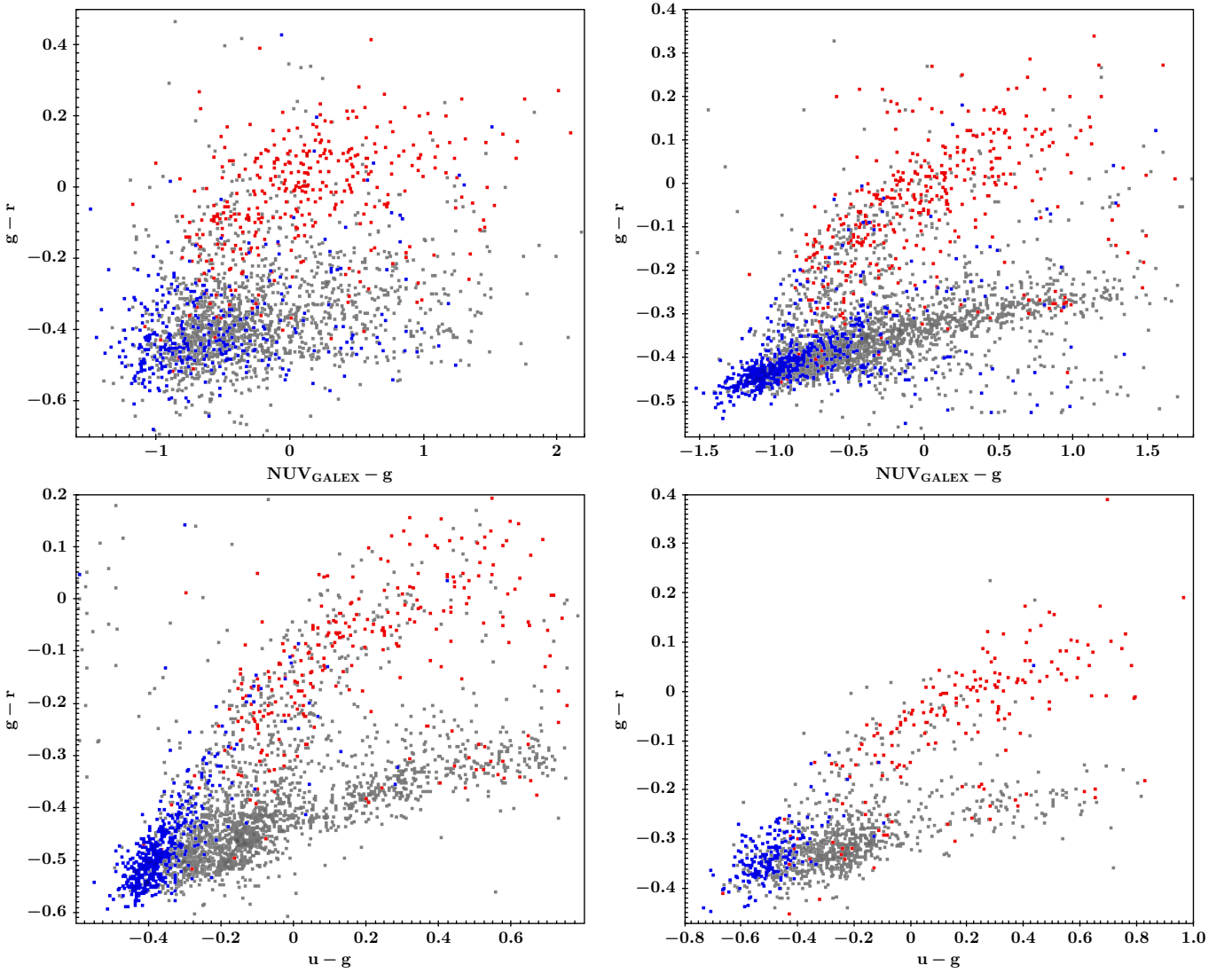


Fig. 4. Colour-colour diagrams of the known, spectroscopically classified sdO/B stars from Geier et al. (2017) catalogue: sdB and sdOB type (grey), sdO type (blue), sdO/B composite binaries with cool main-sequence companions (red). Upper left panel: GALEX/APASS. Upper right panel: GALEX/PS1. Lower left panel: SDSS. Lower right panel: SkyMapper.

1.87 indicating a high quality for all sources. The mean value of `astrometric_excess_noise` is 0.34 ± 0.53 mas and only 2% of the sample have values in excess of 2 mas. Because a significant fraction of the hot subdwarf population are wide binary systems, which should be detectable by *Gaia* in future releases, we refrain from imposing a cut in `astrometric_excess_noise`.

The values of `phot_bp_rp_excess_factor` showed a much wider spread indicating a significant fraction of objects with unreliable photometry. To remove contaminant sources we followed the approach of Gentile Fusillo et al. (2018) and excluded objects with values higher than $1.7 + 0.06 \times (G_{BP} - G_{RP})^2$.

However, in dense regions still contaminant sources remained. This became apparent, when looking at the spatial distribution of objects from the absolute magnitude selected sample. This sample reaches out to distances of about 2 kpc, but still showed overdensities towards the LMC and SMC.

To filter out obviously spurious sources, we calculated a density parameter for all sources as described in Gentile Fusillo et al. (2018). The number of *Gaia* DR2 targets around each source was calculated and converted to a target density

per square degree. For objects with density values higher than 50 000 we applied as stricter quality criterion a parallax uncertainty `e_PLX` better than 10%. The threshold value was adjusted to remove the spurious sources towards the LMC/SMC and at the same time not to exclude too many sources.

Applying all those additional quality filters, we select 39 800 unique sources, which constitute our final *Gaia* catalogue.

3.6. Additional data

To complement the *Gaia* data and the multi-band ultraviolet and optical photometry of the large all-sky surveys, we cross-matched our final *Gaia* catalogue with other recent releases of multi-band photometric catalogues ranging from the optical to the infrared (see Table 4).

Additional optical photometry was obtained from the VST-ATLAS (DR3, Shanks et al. 2015) and the Kilo-Degree (KiDS DR3, de Jong et al. 2015) surveys in the *ugriz*-bands as well as the VST Photometric H_α Survey of the Southern Galactic Plane and Bulge VPHAS+ (DR3, Drew et al. 2014) in the *ugriH α* -

Table 3. Catalogue statistics

Total	39800
Absolute magnitude selection	8760
Reduced proper motion selection	31040
Objects with multi-band photometry	30728

bands and the INT Photometric H_α Survey of the Northern Galactic Plane IPHAS (DR2, Barentsen et al. 2014) in the H_α -bands.

Near Infrared photometry was obtained from the 2MASS All-Sky Catalog of Point Sources (Skrutskie et al. 2006) in the JHK -bands, the UKIRT Infrared Deep Sky Survey (UKIDSS Large Area Survey DR9, Lawrence et al. 2007; UKIDSS-DR6 Galactic Plane Survey, Lucas et al. 2008) in the $YJHK$ -bands, the VISTA Hemisphere Survey (VHS DR5, McMahon et al. in prep.), the VISTA Kilo-degree Infrared Galaxy Survey (VIKING DR4, Edge et al. 2013) in the $ZYJHK_S$ -bands as well as the the Vista Variables in the Via Lactea Survey VVV (DR4, Minniti et al. 2010). Far infrared photometry was obtained from the AllWISE data release (Cutri et al. 2014) in the four WISE-bands.

The Galactic reddening $E(B - V)$ and the Galactic dust extinction A_V from the maps of Schlafly & Finkbeiner (2011) are also provided. Finally, the spectroscopic classifications for the stars in common with Geier et al. (2017) are provided as well.

4. Catalogue properties

The catalogue contains 39 800 unique sources distributed over the whole sky. Only the central parts of the Galactic plane, which are affected by large reddening and absorption and have not been covered by *Gaia* DR2, and the region around the LMC/SMC, which has been removed, are not fully covered (Fig. 5). 31 040 objects have been selected by colour (see Fig. 7 upper left panel) and reduced proper motion. The much cleaner sample selected by colour and absolute magnitude (see Fig. 7 upper left panel) consists of 8760 objects (see Fig. 6, see also Table 3).

To estimate the fraction of stars later than spectral type B, we assume that the multi-band photometry cleaning removes most of those objects. 30 728 objects have sufficient multi-band photometry (Fig. 8) and the remaining 9072 objects are predominantly located in the dense and reddened regions close to the Galactic plane. We estimate the level of contamination in these regions to be around 50% (see Sect. 3.4). This translates into a total contamination fraction of about 11% for the full sample.

To estimate the contamination fraction independently, we crossmatched the catalogue with the SIMBAD database. 4885 objects have classifications in SIMBAD. Only 18 objects have spectroscopic classifications of F or later. 434 objects are classified as A/DA-type corresponding to a fraction of 9%.

We also used the SIMBAD classifications to estimate the number of main-sequence O and B stars in our sample. Stars so classified have been checked against their absolute magnitudes in the G-band, which have now been calculated for stars with parallax measurements better than 30%. Taking into account uncertainties, we assume that O/B-type MS-stars have absolute magnitudes brighter than 1.0 mag (Wegner 2006). Adopting this criterion, we find 53 stars i.e. 1% of the sample. There is also some overlap with the *Gaia* WD catalogue of Gentile Fusillo et al. (2018). A fraction of 4% of our sample is also in the WD cat-

alogue (with probabilities of being WDs exceeding 75%), mostly including objects at the faint end of our magnitude range.

Our *Gaia* catalogue contains 4169 objects or 74% of the hot subdwarf catalogue of Geier et al. (2017). The objects, that are in the catalogue of Geier et al. (2017), but not in our *Gaia* catalogue, are excluded for several reasons. 82% of those objects are either fainter than $G = 19$ mag or redder than $G_{BP} - G_{RP} = -0.05$. The remaining objects are predominantly (fraction of 66%) misclassified WDs with $M_G > 7$ mag. Only 75 objects remain unaccounted for and will be inspected in detail before the next release of the spectroscopic catalogue.

Restricting the hot subdwarf catalogue from Geier et al. (2017) only to single-lined, spectroscopically classified sdO/Bs, 81% are also found in our *Gaia* catalogue. Checking the absolute magnitudes of the stars from the hot subdwarf catalogue, which are not part of the *Gaia* catalogue, we found that about one third of those objects are actually misclassified WDs. Taking this into account, about 90% of the known single sdO/Bs are in our *Gaia* selection.

The *Gaia* G magnitude of a hot subdwarf at 1.5 kpc, would be ~ 17 mag. Down to this magnitude, the parallax precision is usually better than 20%; thus, all the single subdwarfs, above the Galactic plane should be in our *Gaia* catalogue. In the Galactic plane, at ~ 1 kpc we could find an $E(B - V) \sim 1$, which corresponds to ~ 3.5 mag of extinction in the G band, i.e. a hot subdwarf at this distance would be fainter than 19 mag, which is more than allowed by our magnitude limit.

We therefore consider our *Gaia* catalogue to be complete to about 90% for single-lined sdO/B stars at high Galactic latitudes and moderate star densities with a magnitude limit of $G < 19$ mag. The level of completeness close to the Galactic plane should be much lower and cannot really be estimated without spectroscopic follow-up. Our selection is biased against hot subdwarfs with cool MS-companions in composite binaries.

The absolute magnitude selected subsample should also be volume-complete to a similar level up to ~ 1.5 kpc at high Galactic latitudes (see Fig. 9).

5. Conclusions

Based on data from *Gaia* DR2 and several ground-based, multi-band photometry surveys we compiled an all-sky catalogue of 39 800 candidates for hot subluminescent stars. We expect the majority of those objects to be hot subdwarf stars of spectral type B and O, followed by blue horizontal branch stars of late B-type (HBB), hot post-AGB stars, and central stars of planetary nebulae. About 5% of the sample are likely to be WDs or main-sequence stars of spectral-type B and O. About 10% of the sample may be stars cooler than corresponding to spectral type B.

The catalogue is magnitude limited to $G < 19$ mag and covers the whole sky except a small region around the LMC and SMC. Except from the Galactic plane, we expect the catalogue to be fairly complete up to about 1.5 kpc.

In principle, the catalogue can be extended to fainter magnitudes reaching the *Gaia* limit of $G = 20.7$ mag. However, due to much more extreme contamination by faint main-sequence stars and WDs, we will wait for the next *Gaia* releases to do so. The better quality of the astrometry and the availability of the low-res spectrophotometry should make it easier to remove contaminant sources. The same holds for the crowded regions in the Galactic plane. Here also reddening has to be properly corrected for and we expect to take advantage of improved 3D reddening maps before digging deeper into those areas.

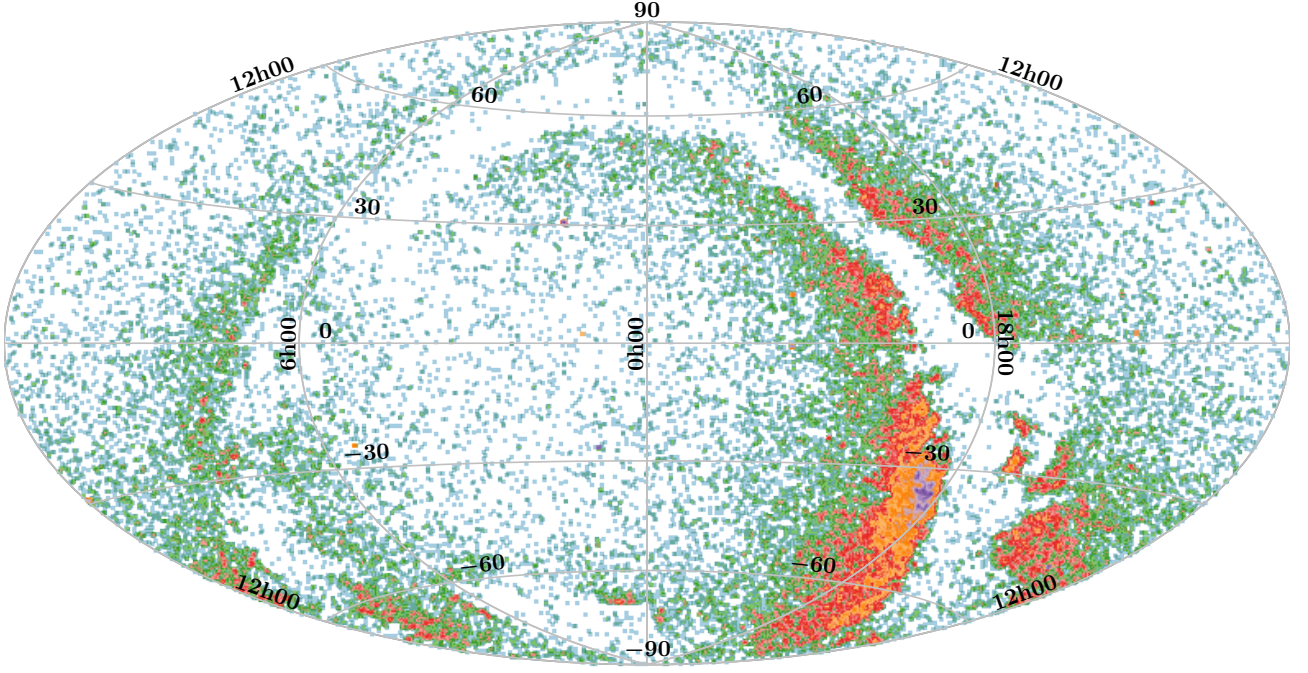


Fig. 5. Sky distribution in equatorial coordinates of the full sample, containing 39 800 stars. The colour scale represents the crowding of stars. The crowding of stars in proximity of the Galactic centre is the main cause of contamination in our sample. The LMC and SMC are largely cut out from our selection.

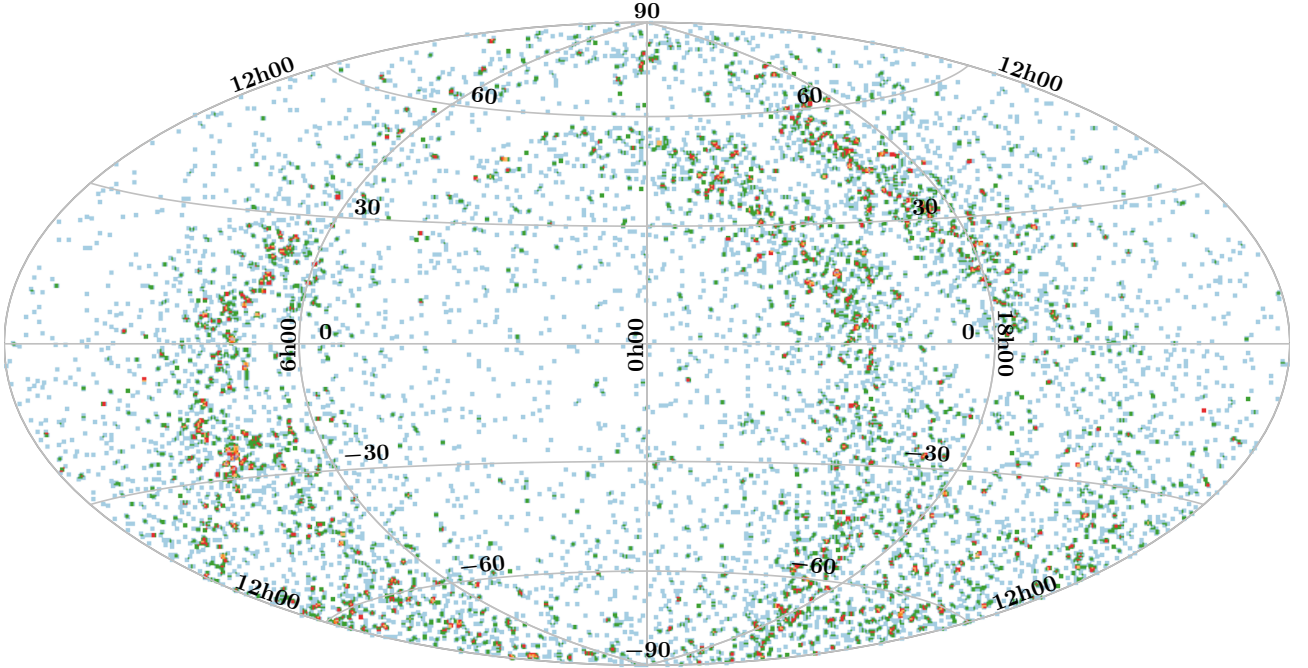


Fig. 6. Sky distribution in equatorial coordinates of the absolute magnitude selected subsample, containing 8760 stars.

The main purpose of this catalogue is to serve as a target list for the large-scale spectroscopic surveys with the next generation of multi-fibre instruments which are ongoing or scheduled to start in the next years (SDSS V, Kollmeier et al.

2017; LAMOST, Luo et al. 2015; WEAVE, Dalton et al. 2012; 4MOST, de Jong et al. 2011; DESI, Levi et al. 2013). The final goal is to obtain spectroscopy of a large fraction of those peculiar types of stars, which is a prerequisite for their proper classifica-

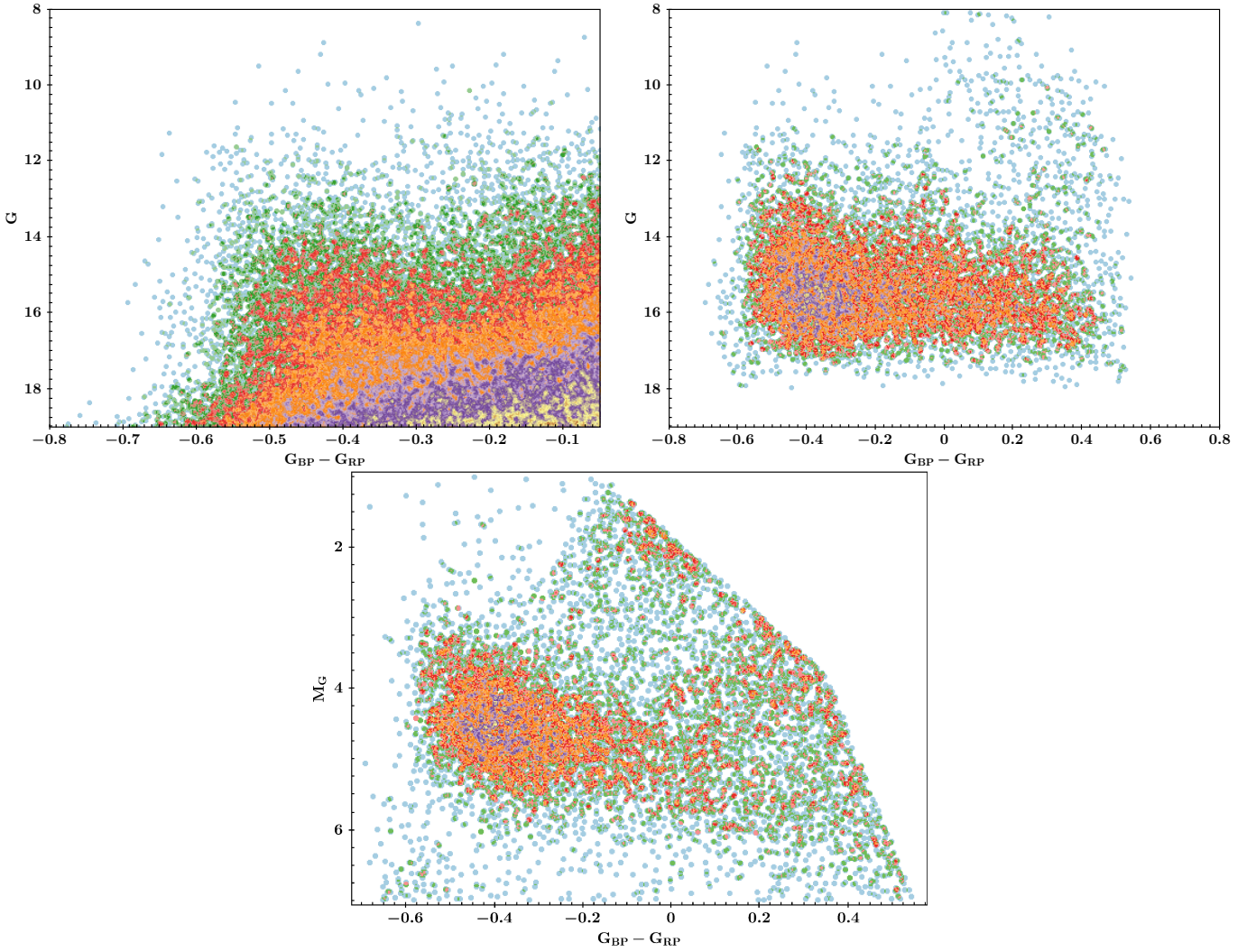


Fig. 7. Upper left panel: *Gaia* colour-magnitude diagram of the reduced proper motion selected sample. Upper right panel: *Gaia* colour-magnitude diagram of the absolute magnitude selected sample. Lower panel: *Gaia* colour-absolute magnitude diagram.

tion, and to study the late stages of stellar evolution based on the population properties of those objects.

Since the catalogue also contains quite a large fraction of yet unknown bright hot subluminal stars (207 sources brighter with $G < 11$ mag, 3406 with $G < 15$ mag not listed in Geier et al. 2017), it is also an important source for large-area time-series photometric surveys looking for close binary stars and stellar pulsations.

We note that especially the absolute magnitude selected subsample, containing 8760 objects, is easily accessible via ground-based spectroscopy and it is a powerful tool for studying the hot subdwarf population. Applying stricter cuts on the area, colours, absolute magnitudes and reduced PMs, cleaner subsamples can be defined.

Acknowledgements. We want to thank the referee Dave Kilkenny for his constructive report and his willingness to review yet another catalogue.

N.G.-F. received funding from the European Research Council under the European Unions Horizon 2020 research and innovation programme n.677706 (WD3D). R.R. acknowledges funding by the German Science foundation (DFG) through grants HE1356/71-1 and IR190/1-1.

This research made use of TOPCAT, an interactive graphical viewer and editor for tabular data Taylor (2005). This research made use of the SIMBAD database, operated at CDS, Strasbourg, France; the VizieR catalog access tool, CDS, Strasbourg, France. Some of the data presented in this paper were obtained

from the Mikulski Archive for Space Telescopes (MAST). STScI is operated by the Association of Universities for Research in Astronomy, Inc., under NASA contract NAS5-26555. Support for MAST for non-HST data is provided by the NASA Office of Space Science via grant NNX13AC07G and by other grants and contracts. This research has made use of the services of the ESO Science Archive Facility.

This work has made use of data from the European Space Agency (ESA) mission *Gaia* (<https://www.cosmos.esa.int/gaia>), processed by the *Gaia* Data Processing and Analysis Consortium (DPAC, <https://www.cosmos.esa.int/web/gaia/dpac/consortium>). Funding for the DPAC has been provided by national institutions, in particular the institutions participating in the *Gaia* Multilateral Agreement.

This publication makes use of data products from the Two Micron All Sky Survey, which is a joint project of the University of Massachusetts and the Infrared Processing and Analysis Center/California Institute of Technology, funded by the National Aeronautics and Space Administration and the National Science Foundation. Based on observations made with the NASA Galaxy Evolution Explorer. GALEX is operated for NASA by the California Institute of Technology under NASA contract NAS5-98034. This research has made use of the APASS database, located at the AAVSO web site. Funding for APASS has been provided by the Robert Martin Ayers Sciences Fund.

Based on observations obtained as part of the VISTA Hemisphere Survey, ESO Program, 179.A-2010 (PI: McMahon). This publication has made use of data from the VIKING survey from VISTA at the ESO Paranal Observatory, programme ID 179.A-2004. Data processing has been contributed by the VISTA Data Flow System at CASU, Cambridge and WFAU, Edinburgh. Based on data products from observations made with ESO Telescopes at the La Silla Paranal Observatory under program ID 177.A 3011(A,B,C,D,E,F). Based on data prod-

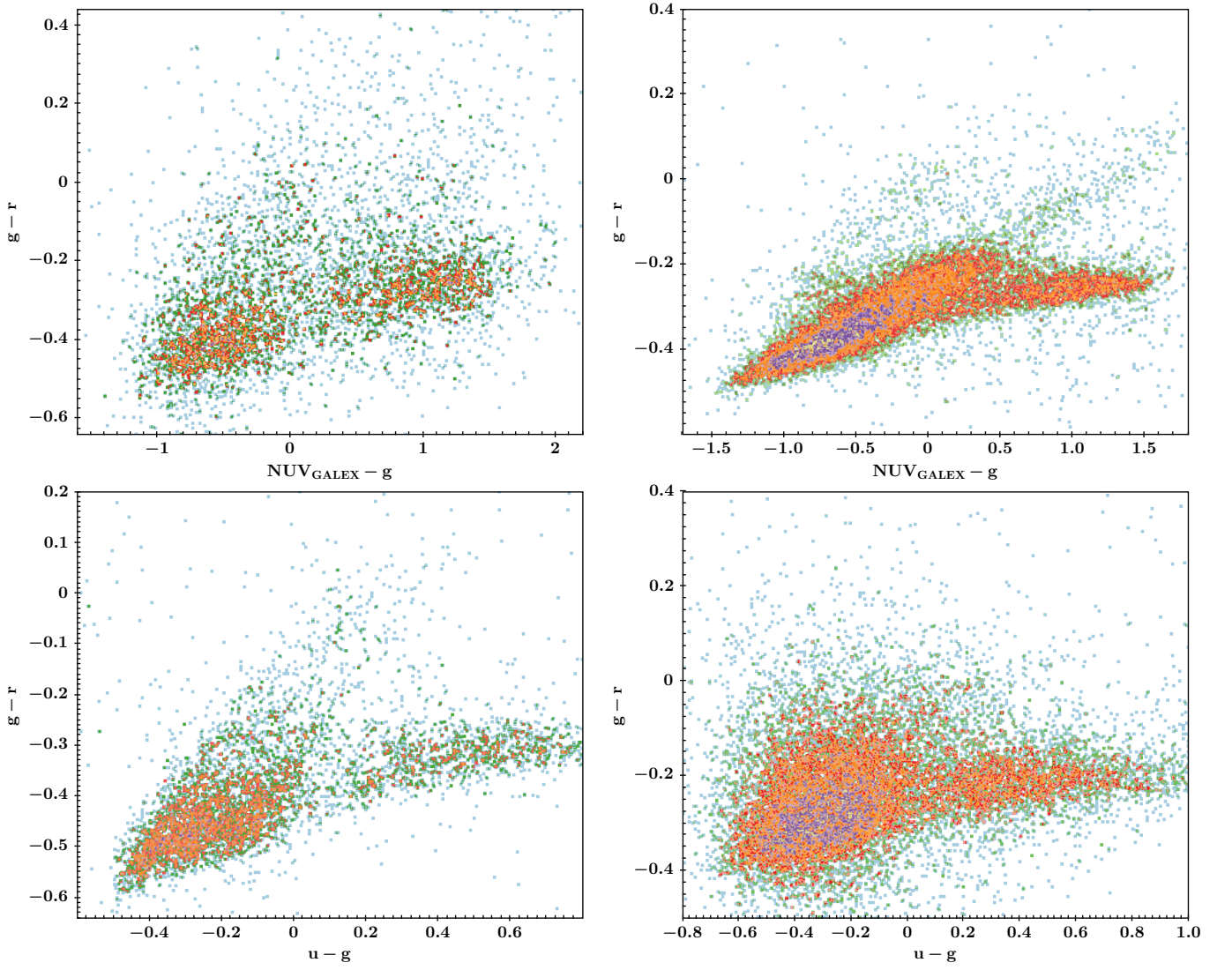


Fig. 8. Colour-colour diagrams of our *Gaia* catalogue. Upper left panel: GALEX/APASS. Upper right panel: GALEX/PS1. Lower left panel: SDSS. Lower right panel: SkyMapper.

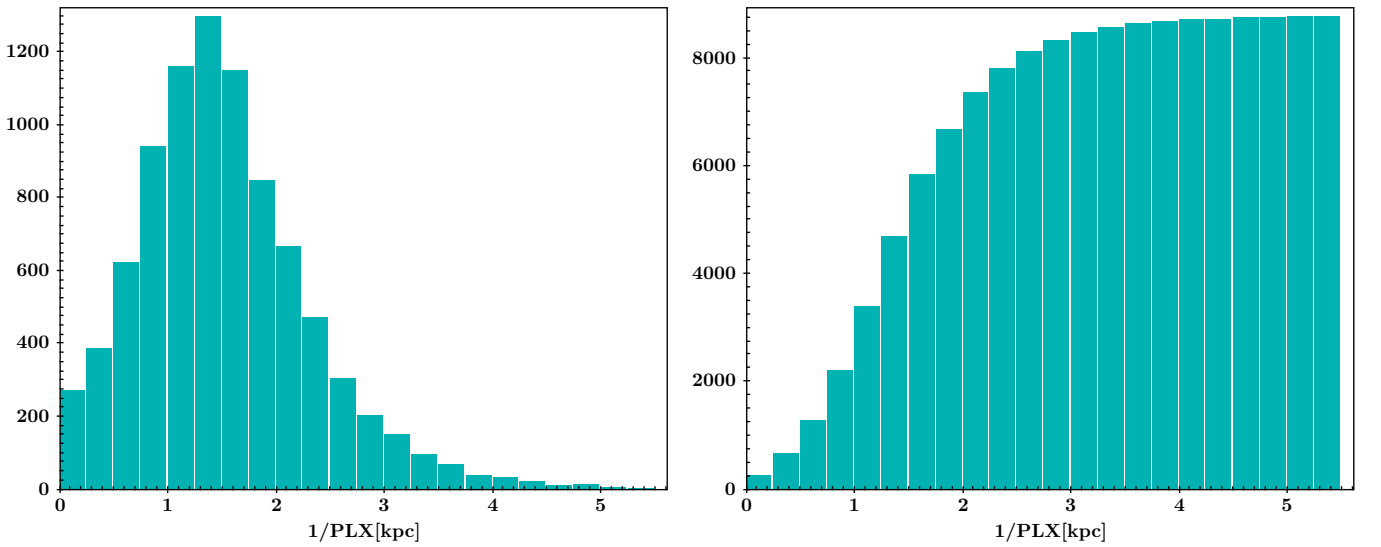


Fig. 9. Left panel: Distance distribution of the absolute magnitude selected sample. Right panel: Cumulative distance distribution.

ucts from observations made with ESO Telescopes at the La Silla Paranal Observatory under programme IDs 177.A-3016, 177.A-3017 and 177.A-3018, and on data products produced by Target/OmegaCEN, INAF-OACN, INAF-OAPD and the KiDS production team, on behalf of the KiDS consortium. OmegaCEN and the KiDS production team acknowledge support by NOVA and NWO-M grants. Members of INAF-OAPD and INAF-OACN also acknowledge the support from the Department of Physics & Astronomy of the University of Padova, and of the Department of Physics of Univ. Federico II (Naples). This publication makes use of data products from the Wide-field Infrared Survey Explorer, which is a joint project of the University of California, Los Angeles, and the Jet Propulsion Laboratory/California Institute of Technology, and NEOWISE, which is a project of the Jet Propulsion Laboratory/California Institute of Technology. WISE and NEOWISE are funded by the National Aeronautics and Space Administration. This paper makes use of data obtained as part of the INT Photometric H Survey of the Northern Galactic Plane (IPHAS, www.iphas.org) carried out at the Isaac Newton Telescope (INT). The INT is operated on the island of La Palma by the Isaac Newton Group in the Spanish Observatorio del Roque de los Muchachos of the Instituto de Astrofísica de Canarias. All IPHAS data are processed by the Cambridge Astronomical Survey Unit, at the Institute of Astronomy in Cambridge. The bandmerged DR2 catalogue was assembled at the Centre for Astrophysics Research, University of Hertfordshire, supported by STFC grant ST/J001333/1. Based on data products from observations made with ESO Telescopes at the La Silla Paranal Observatory under programme ID 177.D-3023, as part of the VST Photometric H Survey of the Southern Galactic Plane and Bulge (VPHAS+, www.vphas.eu).

Funding for the SDSS and SDSS-II has been provided by the Alfred P. Sloan Foundation, the Participating Institutions, the National Science Foundation, the U.S. Department of Energy, the National Aeronautics and Space Administration, the Japanese Monbukagakusho, the Max Planck Society, and the Higher Education Funding Council for England. The SDSS Web Site is <http://www.sdss.org/>. The The Guide Star Catalog-II is a joint project of the Space Telescope Science Institute and the Osservatorio Astronomico di Torino. Space Telescope Science Institute is operated by the Association of Universities for Research in Astronomy, for the National Aeronautics and Space Administration under contract NAS5-26555. The participation of the Osservatorio Astronomico di Torino is supported by the Italian Council for Research in Astronomy. Additional support is provided by European Southern Observatory, Space Telescope European Coordinating Facility, the International GEMINI project and the European Space Agency Astrophysics Division. SDSS is managed by the Astrophysical Research Consortium for the Participating Institutions. The Participating Institutions are the American Museum of Natural History, Astrophysical Institute Potsdam, University of Basel, University of Cambridge, Case Western Reserve University, University of Chicago, Drexel University, Fermilab, the Institute for Advanced Study, the Japan Participation Group, Johns Hopkins University, the Joint Institute for Nuclear Astrophysics, the Kavli Institute for Particle Astrophysics and Cosmology, the Korean Scientist Group, the Chinese Academy of Sciences (LAMOST), Los Alamos National Laboratory, the Max-Planck-Institute for Astronomy (MPIA), the Max-Planck-Institute for Astrophysics (MPA), New Mexico State University, Ohio State University, University of Pittsburgh, University of Portsmouth, Princeton University, the United States Naval Observatory, and the University of Washington.

Funding for SDSS-III has been provided by the Alfred P. Sloan Foundation, the Participating Institutions, the National Science Foundation, and the U.S. Department of Energy Office of Science. The SDSS-III web site is <http://www.sdss3.org/>. SDSS-III is managed by the Astrophysical Research Consortium for the Participating Institutions of the SDSS-III Collaboration including the University of Arizona, the Brazilian Participation Group, Brookhaven National Laboratory, University of Cambridge, Carnegie Mellon University, University of Florida, the French Participation Group, the German Participation Group, Harvard University, the Instituto de Astrofísica de Canarias, the Michigan State/Notre Dame/JINA Participation Group, Johns Hopkins University, Lawrence Berkeley National Laboratory, Max Planck Institute for Astrophysics, Max Planck Institute for Extraterrestrial Physics, New Mexico State University, New York University, Ohio State University, Pennsylvania State University, University of Portsmouth, Princeton University, the Spanish Participation Group, University of Tokyo, University of Utah, Vanderbilt University, University of Virginia, University of Washington, and Yale University.

References

- Alam, S., Albareti, F. D., Allende Prieto, C., et al. 2015, *ApJS*, 219, 12
 Barentsen, G., Farnhill, H. J., Drew, J., et al. 2014, *MNRAS*, 444, 3230
 Bianchi, L., Herald, J., Efremova, B., et al. 2011, *Ap&SS*, 335, 161
 Chambers, K.C., et al. 2016, *arXiv:1612.05560*
 Charpinet, S., van Grootel, V., Fontaine, G., et al. 2011, *A&A*, 530, 3
 Chavira, E. 1958, *Bol. Obs. Tonantz. Tacub.*, 2, 15
 Chavira, E. 1959, *Bol. Obs. Tonantz. Tacub.*, 2, 3
 Cutri, R. M., et al. 2014, *VizieR Online Catalog*, II/328
 Dalton, G., Trager, S. C., Abrams, D. C., et al. 2012, *Proceedings of the SPIE*, 8446
 de Jong, J. T. A., Verdoes Kleijn, G. A., Boxhoorn, D., et al. 2015, *A&A*, 582, 62
 de Jong, R., 2011, *The Messenger*, 145, 14
 Downes, R. A. 1986, *ApJS*, 61, 569
 Drew, J. E., Gonzalez-Solares, E., Greimel, R., et al. 2014, *MNRAS*, 440, 2036
 Edge, A., Sutherland, W., Kuijken, K., et al. 2013, *The Messenger*, 154, 32
 Evans, D. W., Riello, M., De Angeli, F. et al. 2018, *A&A*, 616, 4
 Gaia collaboration 2016, *A&A*, 595, 2
 Gaia collaboration 2018a, *A&A*, 616, 1
 Gaia collaboration 2018b, *A&A*, 616, 10
 Geier, S. 2013, *A&A*, 549, 110
 Geier, S., Nesslinger, S., Heber, U., et al. 2007, *A&A*, 464, 299
 Geier, S., Heber, U., Podsiadlowski, Ph., et al. 2010b, *A&A*, 519, 25
 Geier, S., Hirsch, H., Tillich, A., et al. 2011a, *A&A*, 530, 28
 Geier, S., Schaffenroth, V., Drechsel, H., et al. 2011b, *ApJ*, 731, L22
 Geier, S., Marsh, T. R., Wang, B., et al. 2013, *A&A*, 554, 54
 Geier, S., Fürst, F., Ziegerer, E., et al. 2015a, *Science*, 347, 1126
 Geier, S., Kupfer, T., Heber, U., et al. 2015b, *A&A*, 577, 26
 Geier, S., Østensen, R. H., Nemeth, P., et al. 2017, *A&A*, 600, 50
 Gentile Fusillo, N. P., Gänsicke, B. T., & Greiss, S. 2015, *MNRAS*, 448, 2260
 Gentile Fusillo, N. P., Tremblay, P.-E., Gänsicke, B. T., et al. 2018, *MNRAS*, submitted (*arXiv:1807.03315*)
 Girard, T. M., van Altena, W. F., Zacharias, N., et al. 2011, *AJ*, 142, 15
 Girven, J., Steeghs, D., Heber, U., et al. 2012, *MNRAS*, 425, 1013
 Green, R. F., Schmidt, M., & Liebert, J. 1986, *ApJS*, 61, 305
 Hagen, H.-J., Groote, D., Engels, D., & Reimers, D. 1995, *A&AS*, 111, 195
 Haro, G., & Luyten, W. J. 1962, *Bol. Obs. Tonantz. Tacub.*, 3, 37
 Heber, U. 1986, *A&A*, 155, 33
 Heber, U. 2016, *PASP*, 128, 2001
 Henden, A. A., Templeton, M., Terrell, D., et al. 2016, *VizieR Online Data Catalog*, II/336
 Humason, M. L., & Zwicky, F. 1947, *ApJ*, 105, 85
 Iriarte, B., & Chavira, E. 1957, *Bol. Obs. Tonantz. Tacub.*, 2, 3
 Kawka, A., Vennes, S., O'Toole, S. J., et al. 2015, *MNRAS*, 450, 3514
 Kepler, S. O., Pelisoli, I., Koester, D., et al. 2015, *MNRAS*, 446, 4078
 Kepler, S. O., Pelisoli, I., Koester, D., et al. 2016, *MNRAS*, 455, 3413
 Kilkenny, D., Heber, U., & Drilling, J. S. 1988, *SAOAC*, 12, 1
 Kilkenny, D., O'Donoghue, D., Koen, C., Stobie, R. S., & Chen, A. 1997, *MNRAS*, 287, 867
 Kilkenny, D., O'Donoghue, D., Woters, H. L., et al. 2015, *MNRAS*, 453, 1879
 Kilkenny, D., Woters, H. L., O'Donoghue, D., et al. 2016, *MNRAS*, 459, 4343
 Kollmeier, J., Zasowski, G., Rix, H.-W., et al. 2017 (*arXiv:1711.03234*)
 Kupfer, T., Geier, S., Heber, U., et al. 2015, *A&A*, 576, 44
 Kupfer, T., Korol, V., Shah, S., et al. 2018, *MNRAS*, 480, 302
 Lawrence, A., Warren, S. J., Almaini, O., et al. 2007, *MNRAS*, 379, 1599
 Levi, M., Bebek, C., Beers, T., et al. 2013, *White Paper for Snowmass 2013* (*arXiv:1308.0847*)
 Lindegren, L., Hernandez, J., Bombrun, A., et al. 2018, *A&A*, 616, 2
 Lucas, P. W., Hoare, M. G., Longmore, A., et al. 2008, *MNRAS*, 391, 136
 Luo, A.-L., Zhai, Y.-H., Zhao, G., et al. 2015, *RAA*, 15, 1095
 Luo, Y.-P., Nemeth, P., Liu, C., Deng, L.-C., & Han, Z. 2016, *ApJ*, 818, 202
 Maxted, P. F. L., Marsh, T. R., & North, R. C. 2000, *MNRAS*, 317, L41
 Maxted, P. F. L., Heber, U., Marsh, T. R., & North, R. C. 2001, *MNRAS*, 326, 139
 Michalik, D., Lindegren, L., & Hobbs, D. 2015, *A&A*, 574, 115
 Micaelán, A. M. 2008, *AJ*, 136, 946
 Micaelán, A. M., Nesci, R., Rossi, C., et al. 2007, *A&A*, 464, 1177
 Minniti, D., Lucas, P. W., Emerson, J. P., et al. 2010, *New Astronomy*, 15, 433
 O'Donoghue, D., Kilkenny, D., Koen, C., et al. 2013, *MNRAS*, 431, 240
 Oreiro, R., Rodriguez-Lopez, C., Solano, E., et al. 2011, *A&A*, 530, 2
 Østensen, R. H., 2006, *Baltic Astronomy*, 15, 85
 Østensen, R. H., Silvotti, R., Charpinet, S., et al. 2010b, *MNRAS*, 409, 1470
 O'Toole, S. J., & Heber, U. 2006, *A&A*, 452, 579
 Perez-Fernandez, E., Ulla, A., Solano, E., Oreiro, R., & Rodrigo, C. 2016, *MNRAS*, 457, 3396
 Schlafly, E. F., & Finkbeiner, D. P. 2011, *ApJ*, 737, 103
 Shanks, T., Metcalfe, N., Chehade, B., et al. 2015, *MNRAS*, 451, 4238
 Skrutskie, M. F., Cutri, R. M., Stiening, R., et al. 2006, *AJ*, 131, 1163
 Taylor, M. B. 2005, *ASP Conf. Ser.*, 347, 29
 Vennes, S., Kawka, A., & Németh, P. 2011, *MNRAS*, 410, 2095
 Wegner, W. 2006, *MNRAS*, 371, 185
 Wisotzki, L., Koehler, T., Groote, D., & Reimers, D. 1996, *A&AS*, 115, 227
 Wolf, C., Onken, C. A., Luvaul, L. C., et al. 2018, *PASA*, 35, 10

Table 4. Catalogue columns

Column	Format	Description	Unit
NAME_SIMBAD	A30	Target name (SIMBAD)	
GAIA_DESIG	A30	<i>Gaia</i> designation	
RAJ2000	F10.6	Right ascension (J2000) CDS	deg
DEJ2000	F10.6	Declination (J2000) CDS	deg
RA_ICRS	F10.6	<i>Gaia</i> right ascension ICRS (J2015.5)	deg
DE_ICRS	F10.6	<i>Gaia</i> declination ICRS (J2015.5)	deg
GLON	F10.6	Galactic longitude	deg
GLAT	F10.6	Galactic latitude	deg
SELECTION	A20	Selection method:	
		Colour-absolute magnitude (COLOUR_PLX)	
		Colour-reduced proper motion (COLOUR_REDPM)	
SPEC_SIMBAD	A20	Spectroscopic classification (SIMBAD)	
SPEC_SDCAT	A20	Spectroscopic classification hot subdwarf catalogue	
PLX	F6.4	<i>Gaia</i> parallax	mas
e_PLX	F6.4	Error on PLX	mas
M_G	F6.4	Absolute magnitude in the G-band	mag
e_M_G	F6.4	Error on M_G	mag
G_GAIA	F6.4	<i>Gaia</i> magnitude in the G-band	mag
e_G_GAIA	F6.4	Error on G_GAIA (CDS)	mag
BP_GAIA	F6.4	<i>Gaia</i> magnitude in the BP-band	mag
e_BP_GAIA	F6.4	Error on BP_GAIA (CDS)	mag
RP_GAIA	F6.4	<i>Gaia</i> magnitude in the RP-band	mag
e_RP_GAIA	F6.4	Error on RP_GAIA (CDS)	mag
BP-RP_GAIA	F6.4	BP-RP colour index	mag
PMRA_GAIA	F9.3	<i>Gaia</i> proper motion $\mu_\alpha \cos \delta$	mas yr ⁻¹
e_PMRA_GAIA	F9.3	Error on PMRA_GAIA	mas yr ⁻¹
PMDE_GAIA	F9.3	<i>Gaia</i> proper motion μ_δ	mas yr ⁻¹
e_PMDE_GAIA	F9.3	Error on PMDE_GAIA	mas yr ⁻¹
EB-V	F6.4	Interstellar reddening E(B-V)	mag
e_EB-V	F6.4	Error on EB-V	mag
AV	F6.4	Interstellar extinction A_V	mag
FUV_GALEX	F6.3	GALEX FUV-band magnitude	mag
e_FUV_GALEX	F6.3	Error on FUV_GALEX	mag
NUV_GALEX	F6.3	GALEX NUV-band magnitude	mag
e_NUV_GALEX	F6.3	Error on NUV_GALEX	mag
V_APASS	F6.3	APASS V-band magnitude	mag
e_V_APASS	F6.3	Error on V_APASS	mag
B_APASS	F6.3	APASS B-band magnitude	mag
e_B_APASS	F6.3	Error on V_APASS	mag
g_APASS	F6.3	APASS g-band magnitude	mag
e_g_APASS	F6.3	Error on g_APASS	mag
r_APASS	F6.3	APASS r-band magnitude	mag
e_r_APASS	F6.3	Error on r_APASS	mag
i_APASS	F6.3	APASS i-band magnitude	mag
e_i_APASS	F6.3	Error on i_APASS	mag
u_SDSS	F6.3	SDSS u-band magnitude	mag
e_u_SDSS	F6.3	Error on u_SDSS	mag
g_SDSS	F6.3	SDSS g-band magnitude	mag
e_g_SDSS	F6.3	Error on g_SDSS	mag
r_SDSS	F6.3	SDSS r-band magnitude	mag
e_r_SDSS	F6.3	Error on r_SDSS	mag
i_SDSS	F6.3	SDSS i-band magnitude	mag
e_i_SDSS	F6.3	Error on i_SDSS	mag
z_SDSS	F6.3	SDSS z-band magnitude	mag
e_z_SDSS	F6.3	Error on z_SDSS	mag
u_SKYM	F6.3	SkyMapper u-band magnitude	mag
e_u_SKYM	F6.3	Error on u_SKYM	mag
v_SKYM	F6.3	SkyMapper v-band magnitude	mag
e_v_SKYM	F6.3	Error on v_SKYM	mag
g_SKYM	F6.3	SkyMapper g-band magnitude	mag

e_g_SKYM	F6.3	Error on g_SKYM	mag
r_SKYM	F6.3	SkyMapper r-band magnitude	mag
e_r_SKYM	F6.3	Error on r_SKYM	mag
i_SKYM	F6.3	SkyMapper i-band magnitude	mag
e_i_SKYM	F6.3	Error on i_SKYM	mag
z_SKYM	F6.3	SkyMapper z-band magnitude	mag
e_z_SKYM	F6.3	Error on z_SKYM	mag
u_ATLAS	F7.4	ATLAS u-band magnitude	mag
e_u_ATLAS	F7.4	Error on u_ATLAS	mag
g_ATLAS	F7.4	ATLAS g-band magnitude	mag
e_g_ATLAS	F7.4	Error on g_ATLAS	mag
r_ATLAS	F7.4	ATLAS r-band magnitude	mag
e_r_ATLAS	F7.4	Error on r_ATLAS	mag
i_ATLAS	F7.4	ATLAS i-band magnitude	mag
e_i_ATLAS	F7.4	Error on i_ATLAS	mag
z_ATLAS	F7.4	ATLAS z-band magnitude	mag
e_z_ATLAS	F7.4	Error on z_ATLAS	mag
u_VPHAS	F7.4	VPHAS u-band magnitude	mag
e_u_VPHAS	F7.4	Error on u_VPHAS	mag
g_VPHAS	F7.4	VPHAS g-band magnitude	mag
e_g_VPHAS	F7.4	Error on g_VPHAS	mag
r2_VPHAS	F7.4	VPHAS r-band magnitude (2nd epoch)	mag
e_r2_VPHAS	F7.4	Error on r2_VPHAS	mag
Ha_VPHAS	F7.4	VPHAS Ha-band magnitude	mag
e_Ha_VPHAS	F7.4	Error on Ha_VPHAS	mag
r_VPHAS	F7.4	VPHAS r-band magnitude (1st epoch)	mag
e_r_VPHAS	F7.4	Error on r_VPHAS	mag
i_VPHAS	F7.4	VPHAS i-band magnitude	mag
e_i_VPHAS	F7.4	Error on i_VPHAS	mag
z_VPHAS	F7.4	VPHAS z-band magnitude	mag
e_z_VPHAS	F7.4	Error on z_VPHAS	mag
u_KiDS	F8.5	KiDS u-band magnitude	mag
e_u_KiDS	F8.5	Error on u_KiDS	mag
g_KiDS	F8.5	KiDS g-band magnitude	mag
e_g_KiDS	F8.5	Error on g_KiDS	mag
r_KiDS	F8.5	KiDS r-band magnitude	mag
e_r_KiDS	F8.5	Error on r_KiDS	mag
i_KiDS	F8.5	KiDS i-band magnitude	mag
e_i_KiDS	F8.5	Error on i_KiDS	mag
g_PS1	F7.4	PS1 g-band magnitude	mag
e_g_PS1	F7.4	Error on g_PS1	mag
r_PS1	F7.4	PS1 r-band magnitude	mag
e_r_PS1	F7.4	Error on r_PS1	mag
i_PS1	F7.4	PS1 i-band magnitude	mag
e_i_PS1	F7.4	Error on i_PS1	mag
z_PS1	F7.4	PS1 z-band magnitude	mag
e_z_PS1	F7.4	Error on z_PS1	mag
y_PS1	F7.4	PS1 y-band magnitude	mag
e_y_PS1	F7.4	Error on y_PS1	mag
r_IPHAS	F6.3	IPHAS r-band magnitude	mag
e_r_IPHAS	F6.3	Error on r_IPHAS	mag
i_IPHAS	F6.3	IPHAS i-band magnitude	mag
e_i_IPHAS	F6.3	Error on i_IPHAS	mag
Ha_IPHAS	F6.3	IPHAS Ha-band magnitude	mag
e_Ha_IPHAS	F6.3	Error on Ha_IPHAS	mag
J_2MASS	F6.3	2MASS J-band magnitude	mag
e_J_2MASS	F6.3	Error on J_2MASS	mag
H_2MASS	F6.3	2MASS H-band magnitude	mag
e_H_2MASS	F6.3	Error on H_2MASS	mag
K_2MASS	F6.3	2MASS K-band magnitude	mag
e_K_2MASS	F6.3	Error on K_2MASS	mag
Y_UKIDSS	F6.3	UKIDSS Y-band magnitude	mag
e_Y_UKIDSS	F6.3	Error on Y_UKIDSS	mag
J_UKIDSS	F6.3	UKIDSS J-band magnitude	mag

e_J_UKIDSS	F6.3	Error on J_UKIDSS	mag
H_UKIDSS	F6.3	UKIDSS H-band magnitude	mag
e_H_UKIDSS	F6.3	Error on H_UKIDSS	mag
K_UKIDSS	F6.3	UKIDSS K-band magnitude	mag
e_K_UKIDSS	F6.3	Error on K_UKIDSS	mag
Y_VHS	F8.5	VHS Y-band magnitude	mag
e_Y_VHS	F8.5	Error on Y_VHS	mag
J_VHS	F8.5	VHS J-band magnitude	mag
e_J_VHS	F8.5	Error on J_VHS	mag
H_VHS	F8.5	VHS H-band magnitude	mag
e_H_VHS	F8.5	Error on H_VHS	mag
Ks_VHS	F8.5	VHS Ks-band magnitude	mag
e_Ks_VHS	F8.5	Error on Ks_VHS	mag
Z_VVV	F8.5	VVV Z-band magnitude	mag
e_Z_VVV	F8.5	Error on Z_VVV	mag
Y_VVV	F8.5	VVV Y-band magnitude	mag
e_Y_VVV	F8.5	Error on Y_VVV	mag
J_VVV	F8.5	VVV J-band magnitude	mag
e_J_VVV	F8.5	Error on J_VVV	mag
H_VVV	F8.5	VVV H-band magnitude	mag
e_H_VVV	F8.5	Error on H_VVV	mag
Ks_VVV	F8.5	VVV Ks-band magnitude	mag
e_Ks_VVV	F8.5	Error on Ks_VVV	mag
Z_VIKING	F8.5	VIKING Z-band magnitude	mag
e_Z_VIKING	F8.5	Error on Z_VIKING	mag
Y_VIKING	F8.5	VIKING Y-band magnitude	mag
e_Y_VIKING	F8.5	Error on Y_VIKING	mag
J_VIKING	F8.5	VIKING J-band magnitude	mag
e_J_VIKING	F8.5	Error on J_VIKING	mag
H_VIKING	F8.5	VIKING H-band magnitude	mag
e_H_VIKING	F8.5	Error on H_VIKING	mag
Ks_VIKING	F8.5	VIKING Ks-band magnitude	mag
e_Ks_VIKING	F8.5	Error on Ks_VIKING	mag
W1	F6.3	WISE W1-band magnitude	mag
e_W1	F6.3	Error on W1	mag
W2	F6.3	WISE W2-band magnitude	mag
e_W2	F6.3	Error on W2	mag
W3	F6.3	WISE W3-band magnitude	mag
e_W3	F6.3	Error on W3	mag
W4	F6.3	WISE W4-band magnitude	mag
e_W4	F6.3	Error on W4	mag
DENSITY	F11.3	Density parameter	
GAIA_Astrometric_EXCESS_NOISE	F8.5	<i>Gaia</i> astrometric_excess_noise parameter	
GAIA_Astrometric_EXCESS_NOISE_SIG	F8.5	<i>Gaia</i> astrometric_excess_noise significance parameter	
GAIA_Astrometric_SIGMA_5D_MAX	F8.5	<i>Gaia</i> astrometric_sigma_5D_max parameter	
GAIA_Phot_BP_RP_EXCESS_FACTOR	F8.5	<i>Gaia</i> phot_BP_RP_excess_factor parameter	